

# Experimental and numerical study of ventilated supercavitation around a cone cavitator

S. Morteza Javadpour<sup>1</sup> · Said Farahat<sup>1</sup> · Hossein Ajam<sup>2</sup> · Mahmoud Salari<sup>3</sup> · Alireza Hossein Nezhad<sup>1</sup>

Received: 24 November 2015 / Accepted: 9 August 2016 / Published online: 15 September 2016  
© Springer-Verlag Berlin Heidelberg 2016

**Abstract** In this paper, a numerical and experimental analysis of the ventilated super-cavitating flow around a cone cavitator is presented. For the first time, the experiments are conducted in an open loop water tunnel. The fluid flow velocity in the test section is between 24 and 37 m/s at a constant rate of injection. The simulations of ventilated supercavitation are provided at different velocities. The corresponding governing equations are solved numerically using the finite element method and the mixture model. Finally, the effect of significant parameters such as cavitation number, inlet velocity on drag coefficient and the shape of cavity are investigated. A comparison of the numerical and experimental results shows that the numerical method can accurately simulate the physics of the ventilated cavitation phenomenon such as the cavity shape. According to the results, the maximum cavity diameter and length declines as the cavitation number increases. With an increase in the flow velocity, the cavity length and diameter increased to 200 and 18 % respectively. At constant rate of the ventilated air, with an increase of cavitation number from 0.15 to 0.25, the drag force drops by 62 %.

## 1 Introduction

When the pressure in a liquid flow falls below the particular saturation vapor pressure, the liquid evaporates. This phenomenon, known as cavitation, has several applications in the industry, and is categorized by a dimensionless cavitation number  $\sigma$ . Supercavitation is the extreme form of cavitation, in which a single bubble of gas is formed around a body moving rapidly through water, such as a projectile. It can significantly reduce the drag of an underwater body, thus enabling a dramatic increase in its maximum speed. When supercavitation occurs on an underwater body, the skin friction drag is reduced drastically, so the supercavitating body can reach higher speeds under water with the same amount of energy spent compared to the absence of supercavitation.

Supercavitation can be divided into natural supercavitation and ventilated supercavitation. The natural supercavitation occurs when the free stream velocity is increased above a certain limit ( $U > 45$  m/s at sea level, and increases with submersion depth (or  $p\infty$ ). This phenomenon can also be achieved by decreasing the ambient pressure,  $p\infty$ , which is only feasible in cavitation tunnels. Increasing the cavity pressure,  $p_c$ , through ventilation of the cavity is called artificial or ventilated supercavitation. The static hydrodynamic forces and cavity shape associated with a given cavitator have been modeled by a number of researchers. Further, drag reduction can be observed on bodies surrounded fully or partially by a natural or gas-ventilated cavity [1].

In the past decade, several researchers have experimentally investigated supercavitating flows. Most of these studies focused on cavitation shape, velocity and pressure distributions of flow field and control and stability of the supercavitating vehicles. Zhang et al. [2] performed a series

✉ Said Farahat  
Farahat@hamoon.usb.ac.ir

<sup>1</sup> Department of Mechanical Engineering, University of Sistan and Baluchestan, P. O. Box: 98155-987, Zahedan, Iran

<sup>2</sup> Department of Mechanical Engineering, Ferdowsi University of Mashhad, Mashhad, Iran

<sup>3</sup> Department of Mechanical Engineering, Imam Hossein University, Tehran, Iran

of projectile and closed-loop water-tunnel experiments to study the shape properties of natural and ventilated supercavitation. They obtain empirical formulas for ventilated cavity shape and cavitation number under zero incidence conditions. Wosnik et al. [3] measured the amount of ventilation gas required for sustaining an artificial cavity at different velocities and velocity distribution in cavitation wake based on the DSPI and PIV techniques. Savchenko [4] investigated the effect of gravity and leakage rate on the shape of ventilated supercavitation through water tunnel experiments. The behavior of supercavitating and cavitating flow around a conical body of revolution with and without ventilation at several angles of attack was studied experimentally by Feng et al. [5]. They demonstrated that the presence of supercavity under the ventilation condition reduced the drag. Natural and ventilated cavitations generated on a smooth-nosed axisymmetric body were studied experimentally by Feng et al. [6].

In recent years, most studies on supercavitating flows have been carried out using numerical methods. Ji and Luo [7] investigated both natural and ventilated cavitation numerically using the solver of a commercial CFD code CFX. They just simulated the cavitating flow around an under-water vehicle under different cavitation conditions. Nesteruk [8] simulated the unsteady evolutions of the slender axisymmetric ventilated supercavity using one-dimensional inviscid flow of the incompressible gas in the channel between the cavity surface and the body of revolution. It was shown that the cavity shape depended strongly on the values of the ventilation rate and the cavitation number. Ventilating supercavities were studied both numerically and experimentally by Rashidi et al. [9]. The simulations were conducted for two different algorithms in free-surface treatment, both using the VOF method, but only one uses Young's algorithm in the advection of the free surface. They showed that the numerical method using Young's algorithm can accurately simulate the physics of ventilated cavitation phenomena such as the cavity shape, gas leakage and re-entrant jet. The shape of ventilated cavity and underwater body drag have been numerically simulated using the commercial code Fluent by Li-Ping et al. [10]. They showed that total drag coefficient can be increased to a minimum value while the ratio of cavity thickness to body's diameter is about 0.02.

Javadpour et al. [11] experimentally investigated important natural supercavitation parameters in an open water tunnel complemented by a numerical analysis with the CFX software. They found a good agreement between the numerical and experimental results. The unsteady simulation of cavitation around NACA 0015 was investigated by Asnaghi et al. [12]. For multiphase simulation, single-fluid Navier–Stokes equations, along with a volume fraction transport equation were employed. For discretization of equations, they used the finite-volume approach written on a

body fitted curvilinear coordinates on collocated grid. Baradaran fard and Nikseresht [13] were investigated unsteady turbulent cavitating flows around a circular disk and a cone cavitator. They have used in a finite volume approach to promote robust solution for unsteady turbulent cavitating flows. Ji and Luo [14] studied natural and ventilated cavitation around an underwater vehicle. They used  $k - \omega$  SST turbulence model and for convenience, the solver of a commercial CFD code CFX coupled with the proposed cavitation model. They showed that for the natural and ventilated cavitation simulation, the predicted cavitation characteristics including the cavity length, cavity diameter and cavity shape agrees satisfactorily with the analytic and experimental results. Jian-hong et al. [15] investigated the multiphase cavitating flow around an underwater projectile. They applied a mixture model to simulate the multiphase cavitating flow including ventilated cavitation caused by air injection as well as natural cavitation. They showed that the drag coefficient is also hardly influenced by the natural cavitation numbers as the gas flow rate is greater than 0.555. The unsteady cavitating flows around the Clark-Y hydrofoil at velocity of 10 m/s are studied by Haung and Wang [16]. They showed that the unsteady cavity shapes and velocity distributions are better consistent with experimental visualizations as compared with the RANS model. Zou et al. [17] investigated the gas-leakage rate of an unsteady ventilated supercavitating body. They calculated the rate of volume change of supercavity based on Logvinovich's principle and the empirical formula and compared the simulation results with the results from experiment.

Most experimental studies on supercavitation have been performed in a closed-loop water tunnel [2, 5, 9, 18–20] and this investigation is the only one that studies ventilated supercavitation flow in an open circuit water tunnel. Also, most studies were conducted to obtain detail information about the cavity shape at a constant velocity [2, 5, 9, 14]. In this study, however, important supercavitation parameters including the cavity shape, formation and the drag coefficient of the cavitator are investigated experimentally in an open water tunnel along with a numerical analysis using the finite element method. This experimental research is accompanied with the numerical modelling.

The paper is organized as follows: first, a description of the physical problem is presented, followed by an experimental and numerical analysis. Then, the experimental and computational results are presented and discussed. Finally, a summary is given and the conclusions are drawn.

## 2 Experimental set-up

The experiments were conducted in a water tunnel located at the Marine Research Center of Iran. The tunnel is a

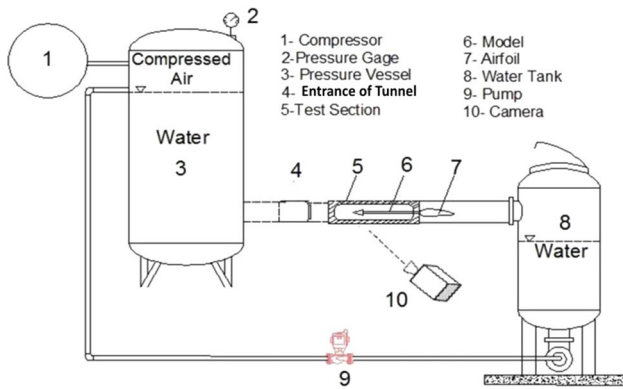


Fig. 1 The schematic view of the water tunnel. The figure is not scale

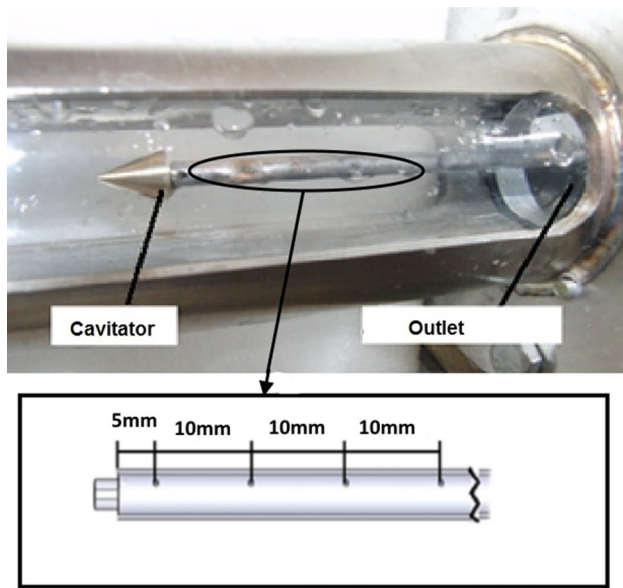


Fig. 2 Test section of water tunnel

semi-open loop water tunnel which is capable of generating velocities up to 40 m/s. The water tunnel is equipped with a computer system, control system, high-speed data collection analyzer and high-speed photograph camera. A model with a nose and cylindrical body is selected without any fin, or other control surface being mounted on it. A schematic view of the components of the water tunnel is shown in Fig. 1.

The cavitation generated on a symmetric cone is investigated based on experimental observations carried out in a water tunnel. Figure 2 shows the test section, where a cone cavitator is placed. The test section is cylindrical with an internal diameter of  $D$  and a length of  $5D$  (Fig. 3). The internal wall of test section is made of Plexiglas with a highly smooth surface. The end part of the test section is at the atmospheric pressure and the water is discharged into an open tank. This water tunnel includes a cylindrical tank which is filled with water injected by the pressurized air to

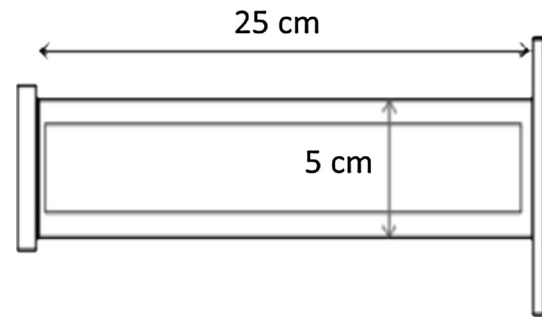


Fig. 3 Dimension of test section

a certain height. Depending on the speed, the air pressure injected for each test is variable. The installed model with a maximum diameter of  $d$  is attached to a dynamometer which is outside the test section by a cylindrical body. The cavitator geometry is shown in Fig. 2. The cavitator diameter is 10 mm, the cone length of  $y_0$  is determined based on the cone angle and the Froude number ( $Fr$ ) varies from 33 to 53 relative to the free-stream velocity.

The water tunnel is equipped with seven pressure sensors to measure the flow pressure. Five of these sensors are installed on the cylindrical body of the model (Fig. 2) and the other two are mounted on the test section (P6) and the water tank (P7). The accuracy of sensors is  $2 \pm 0.01$  bar. Sensors output is converted into digital codes via an A/D convertor card, which is finally recorded. It should be noted that the data frequency of ultimate vector in experiments is 1000 Hz for all sensors. Cavitation profile formed around the cavitator is recorded by a high-speed camera with a frame rate of 600 fps.

To measure drag force, a load cell of 5 kg f was mounted in the standard airfoil out of the test section. Also, load cell and pressure sensor wires were driven out of the water tunnel via this airfoil.

Before conducting the water tunnel tests, the results of cavity shape on a flat disk are compared with the work of Franc and Michel [21]. In Fig. 4, the results of the study about the dimensionless cavity length ( $L_c/d$ ) against the cavitation number of flow have been compared with the experimental data of France and Michel. As can be seen, the results are consistent with experimental data. The results indicate a maximum of 12 % difference between this experiment and Reichardt’s theory and a maximum of 8 % difference with other studies. According to Eq. (1), the theoretical value of the blockage cavitation number is 0.211, whereas the minimum value of cavitation number at the maximum velocity of tests is about 0.25. Considering that  $\sigma_{blockage} < 0.25$  the effect of blockage on the measured drag coefficient and cavity shape is negligible in this experiment.

$$\sigma_{blockage} = \frac{S_u^2}{S_d^2} - 1.0 \tag{1}$$

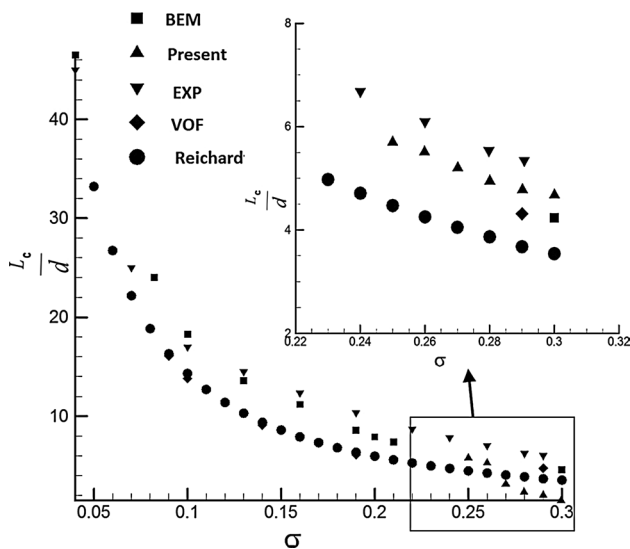


**Fig. 4** Comparison of the present experimental results with those of Reichardt [21]

where  $S_u$  and  $S_d$  stand for the cross-sectional areas of the upstream and downstream regions of the liquid flow respectively.

One of fundamental dimensionless parameters for natural supercavities is Froude number,  $Fr = U_\infty / (gD)^{1/2}$ . Froude number varies from 44.7 to 59 with a cavitation number between 0.25 and 0.36. Semenenko [22], citing Logvinovitch (1973), states that the effect of gravity can be significant if  $\sigma Fr < 2$ . The present application does not require the inclusion of gravity effects.

### 3 Mathematical models

#### 3.1 Governing equations

In this study, a mixture-type multiphase-flow model, based on the isotropic hypothesis for the fluid, along with the averaged Navier–Stokes equations are employed. The equations related to the mass and momentum conservation are solved to obtain the velocity and pressure fields. The mass, momentum, and volume fraction equations can be written as:

$$\frac{\partial \rho_m}{\partial t} + \frac{\partial}{\partial x_i} (\rho_m u_i) = 0 \tag{2}$$

$$\begin{aligned} \frac{\partial}{\partial t} (\rho_m u_i) + \frac{\partial}{\partial x_j} (\rho_m u_i u_j) \\ = -\frac{\partial P}{\partial x_i} + \frac{\partial}{\partial x_j} \left[ \mu_m \left( \frac{\partial u_i}{\partial x_j} + \frac{\partial u_j}{\partial x_i} \right) \right] + \frac{\partial}{\partial x_j} (\tau_{ij}) \end{aligned} \tag{3}$$

where  $u$  and  $P$  are velocity and pressure respectively. The Reynolds stress can be modeled by Boussinesq hypothesis [11] using the following equation:

$$\tau_{ij} = \mu_t \left( \frac{\partial u_i}{\partial x_j} + \frac{\partial u_j}{\partial x_i} \right) - \frac{2}{3} \left( \rho k + \mu_t \frac{\partial u_k}{\partial x_k} \right) \delta_{ij}, \tag{4}$$

where  $\delta_{ij}$  is Kronecker symbol and  $\mu_t$  is the turbulent viscosity.

Among turbulence models, shear stress transport (SST)  $k-\omega$  turbulence model is able to provide accurate predictions under adverse pressure gradients and separating flow [23]. Also, most researchers [14, 18, 24] have used turbulence model of SST to simulate cavitation. Therefore, this model is chosen as the turbulence model for the cavitation simulation in this paper.

The mixture density  $\rho_m$  and viscosity  $\mu_m$  are defined by:

$$\rho_m = \alpha_v \rho_v + \alpha_g \rho_g + (1 - \alpha_v - \alpha_g) \rho_l \tag{5}$$

$$\mu_m = \alpha_v \mu_v + \alpha_g \mu_g + (1 - \alpha_v - \alpha_g) \mu_l \tag{6}$$

where  $\alpha$  is the volume fraction of one component. The subscripts  $v, g$  and  $l$  refer to the components of the vapor, non-condensable gas and liquid respectively.

A cavitation process is governed by the mass transfer equations. Equation (7) gives the conservation equation of vapor volume fraction, and Eq. (8) shows the conservation equation of gas volume fraction.

$$\frac{\partial}{\partial t} (\rho_v \alpha_v) + \frac{\partial}{\partial x_i} (\rho_v \alpha_v u_i) = \dot{m}^- - \dot{m}^+ \tag{7}$$

$$\frac{\partial}{\partial t} (\rho_g \alpha_g) + \frac{\partial}{\partial x_i} (\rho_g \alpha_g u_i) = 0 \tag{8}$$

The domain of problem and boundary conditions are shown in Fig. 5. The velocity components, volume fractions, turbulence intensity and length scale are specified at the velocity inlet boundary and extrapolated at the pressure outlet boundaries.

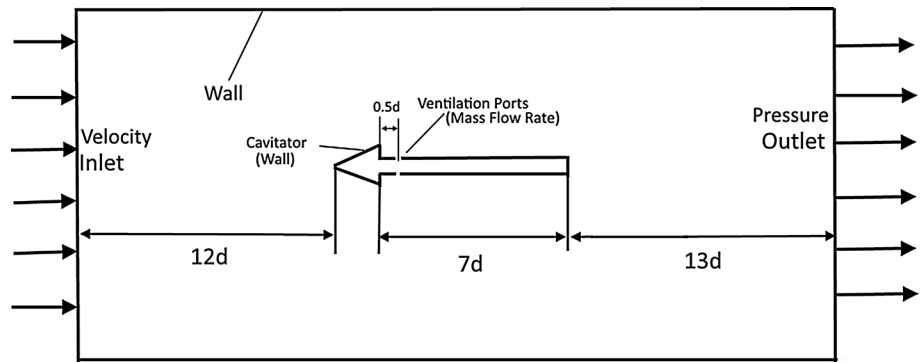
The pressure and volume fractions on walls are extrapolated and the no-slip boundary condition or free-slip boundary is specified. The mass flow rate boundary is defined at the blowhole (injection). The volume fraction of water is assumed one and other phase is considered zero as initial conditions. This means that the entire volume is filled with water.

The non-dimensional parameters of interest are defined as:

$$\sigma_v = \frac{P_\infty - P_v}{\frac{1}{2} \rho U^2} \tag{9}$$

$$\sigma_c = \frac{P_\infty - P_C}{\frac{1}{2} \rho U^2} \tag{10}$$

**Fig. 5** Boundary condition and domain extent



$$C_d = \frac{F_d}{1/2\rho U^2 A} \tag{11}$$

$\rho$  is water density,  $U_\infty$  is inflow velocity,  $P_v$  is water vapor pressure at ambient temperature,  $P_\infty$  is flow pressure,  $P_c$  is the pressure of cavitation,  $\sigma_v$  is natural cavitation number,  $\sigma_c$  is ventilated cavitation number and  $C_d$  is drag coefficient.

### 3.2 Cavitation model

In this study, a “two-phase mixture” approach is introduced by local vapor volume. It has the spatial and temporal variation of the vapor function, which is described by the transport equation and source terms for the mass transfer rate between two phases. The notable advantage of this model is rooted in the convective character of equation, which can significantly contribute to the reproduction of the physics of cavitating flows, such as cavity detachment and cavity closure, and therefore allows modeling the impact of inertial forces and drift of bubbles.

Numerical models of cavitation differ in terms of mass transfer term  $\dot{m}$ . The most common semi-analytical models are Singhal cavitation model [25], Merkle model [26], Schnerr and Sauer model [27] and Kunz model [28]. In the present study, the cavitation model developed by Singhal et al. has been adopted. Source terms included in the transport equation define vapor generation (liquid evaporation) and vapor condensation, respectively. Source terms are a variable of local flow conditions (static pressure and velocity) and fluid properties (liquid and vapor phase densities, saturation pressure and liquid vapor surface tension). The source terms are derived from the Rayleigh-Plesset equation, and high-order terms and viscosity terms are adapted from Singhal et al.

They are given by:

$$\dot{m}^+ = C_{evap} \frac{V_{ch}}{\sigma} \rho_l \rho_v \left[ \frac{2 p_v - p}{3 \rho_l} \right]^{1/2} \frac{\rho_l \alpha_l}{\rho_m} \tag{12}$$

$$\dot{m}^+ = C_{cond} \frac{V_{ch}}{\sigma} \rho_l \rho_v \left[ \frac{2 p - p_v}{3 \rho_l} \right]^{1/2} \frac{\rho_v \alpha_v}{\rho_m} \tag{13}$$

where  $C_{evap} = 0.02$ ,  $C_{cond} = 0.01$  and  $V_{ch} = \sqrt{k p_v}$  and  $\sigma$  and  $k$  denotes the saturated pressure of liquid, surface tension and turbulence energy, respectively.

### 4 Numerical method

The numerical simulation (Ansys CFX 14) can be used to detect cavitation in cavitation flow around cone cavitator. It is important to note that Ansys CFX uses the CV-FEM (control volume-finite element method) method, and the CV-FEM method with the hexahedral mesh outperforms the tetrahedral model, which tends to degrade the computing efficiency.

With the inclusion of CV-FEM method in Ansys CFX 14, the linearized momentum and mass equations can be solved simultaneously with an algebraic multi-grid method based on the additive correction multi-grid strategy. The high-resolution scheme is adopted in space discretization to solve the differential equation, with the second-order space accuracy.

In this paper, several basic hypothesis have been assumed as follows: (1) buoyancy of bodies in water is assumed negligible, (2) gravity is assumed negligible, (3) fluid is considered as incompressible, (4) slip velocity between gas phase and liquid phase is assumed negligible, (5) vapor cavitation due to lower velocity field is assumed negligible.

### 5 Grid independency study

To demonstrate the grid independency of the results, grids similar to that of Fig. 6 are used. Then, length and diameter cavity fractions are calculated and plotted in Fig. 7 at four different nodes ( $N = 420,000$ ,  $N = 920,000$ ,  $N = 1,180,000$

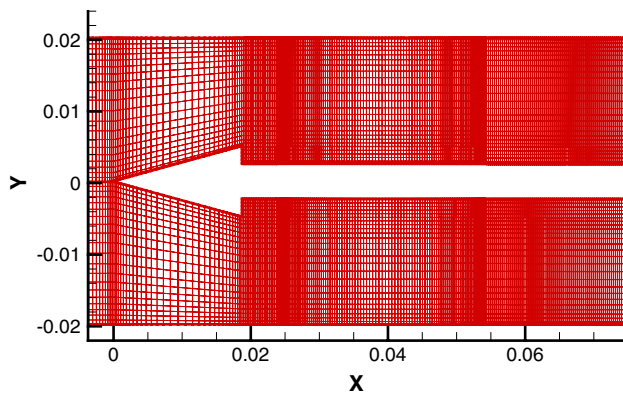


**Fig. 6** Mesh near the cavitator

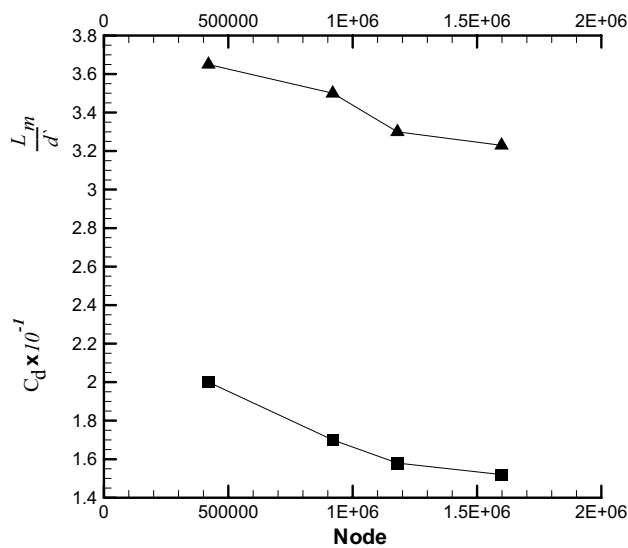


**Fig. 7** Variations of length and diameter of cavity fractions at four different nodes

and  $N = 1,652,000$  nodes). Since the variation between the two grids is small, a grid with  $N = 1,180,000$  nodes is chosen for the present study. In total domain, a structural grid with 1,180,000 nodes is formed.

## 6 Result and discussion

In Fig. 8, the change of Froude number with cavitation number is shown. Changes of cavitation number versus Froude number are linear. The results indicate that the cavitation number drops as Froude number rises. In this paper, the ventilated cavitation experiment is conducted on a  $30^\circ$  cavitator and the cavity shape and drag coefficient of tests are presented.

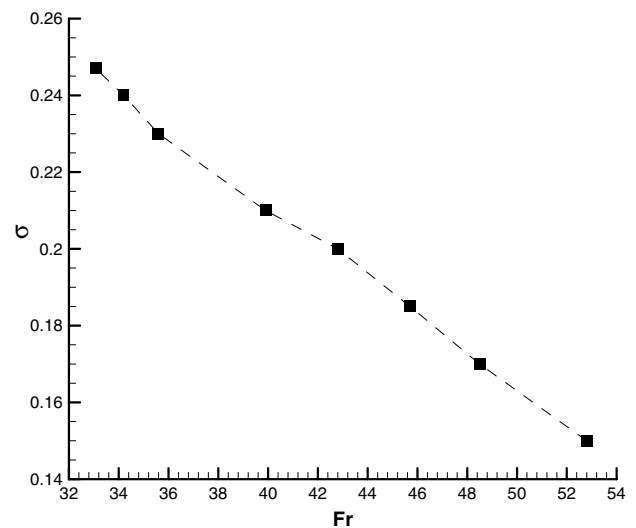


**Fig. 8** Variation of cavitation number with Froude number

### 6.1 Shape of cavity

Figure 9 shows the effect of velocity variations on cavity shape in a  $30^\circ$  cavitator. The flow velocities are in the range of 28–37 m/s. For air ventilation, four ports are used around the slender body at 0.5  $d$  from the leading edge of cavitator. In this study, the ventilation flow rate is 0.0851 l/s with the results indicating the significant effect of velocity on the cavity length.

In Fig. 10, the streamlines around the  $30^\circ$  cavitator and the volume fraction contours are shown for the cavitation number of 0.23. As can be seen, the cavity pressure is constant but where the cavity is closed, the pressure increases to the maximum level, and then declines gradually. In this way, the length of cavity can be estimated. For instance, when the flow velocity is 30 m/s, the cavity length will be 41 mm (Fig. 11).

Figures 12 and 13 show the dimensionless supercavity length and diameter, which compare the results of the numerical method with experimental tests. In both figures, a good agreement was observed between the numerical results and those of experiments with a maximum of 6 % difference. The results show that at low velocities, the effect of ventilation on length and diameter of cavity is insignificant.

The experimental and numerical results indicate that with an increase in the Froude number, the maximum cavity diameter rises initially and then remains at a nearly constant level (Fig. 13).

At  $v < 29$  m/s, the end of the cavity is closed. In the ventilated cavitation after cavity closure, the length and diameter of cavity are less dependent on flow velocity. In this state, the rate of ventilated air is especially effective.

**Fig. 9** Ventilated cavity results on a 30° cavitator in the water tunnel at different velocities

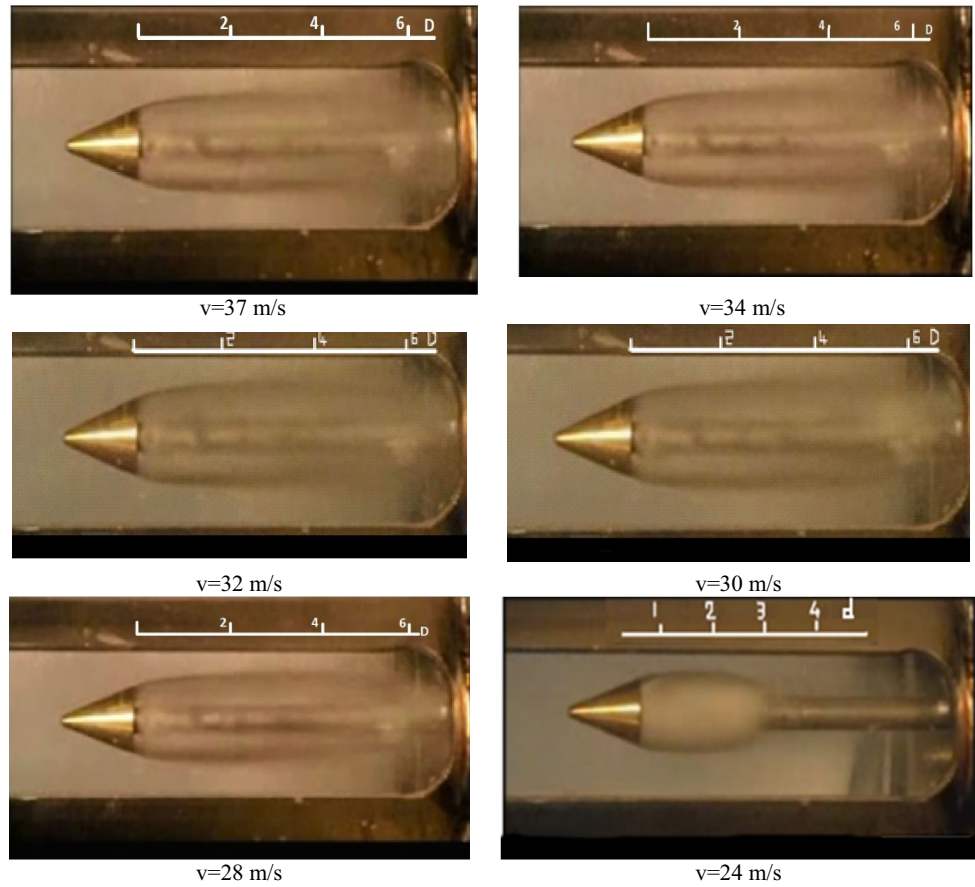
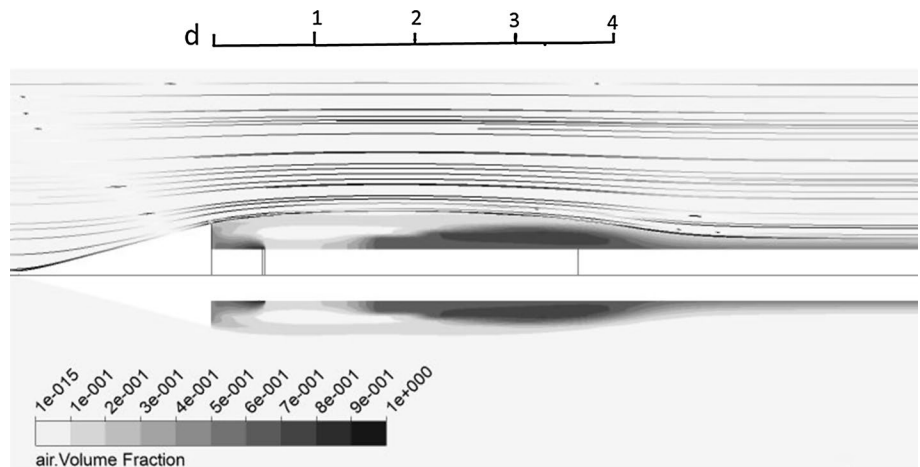


**Fig. 10** Streamlines and air volume fraction contours



Given the practical importance of circular disks, experimental data and theoretical methods have been the subject of extensive studies. To evaluate the present results, the Reichardt’s semi-empirical relations are selected as non-dimensional characteristics of the cavity. The related formulas for these characteristics are given in Eqs. (14)–(16). The cavitation number is the main factor in these formulas [21].

$$\frac{L}{D} = \frac{\sigma_v + 0.008}{\sigma_v(1.7\sigma + 0.066)} \left(\frac{D}{d}\right) \tag{14}$$

$$\frac{D}{d} = \left[ \frac{C_D}{\sigma_v(1 - 0.132\sigma_v^{0.5})} \right]^{0.5} \tag{15}$$

$$C_D = C_{D0}(1 + \sigma_v) \tag{16}$$

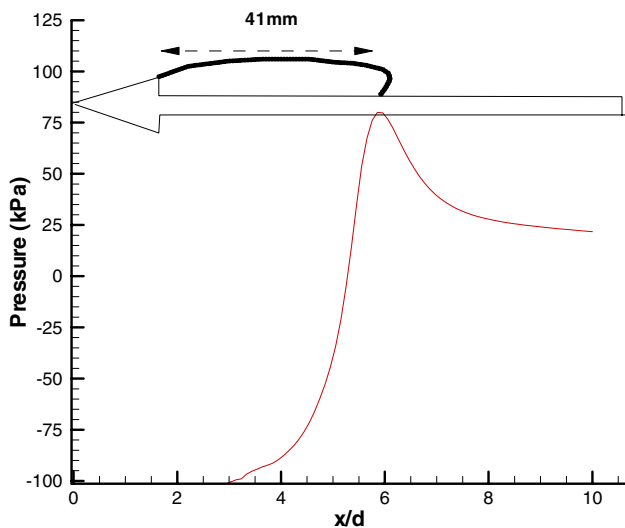


Fig. 11 distribution pressure behind cavitator at  $v = 30$  m/s

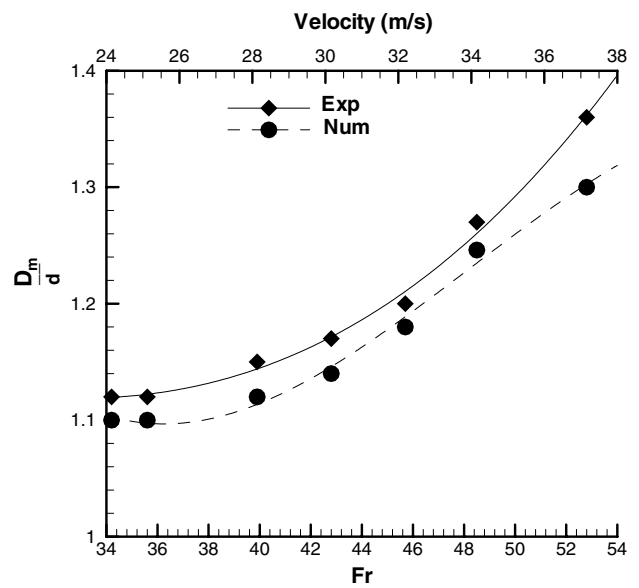


Fig. 13 Dimensionless cavity diameter versus Froude number

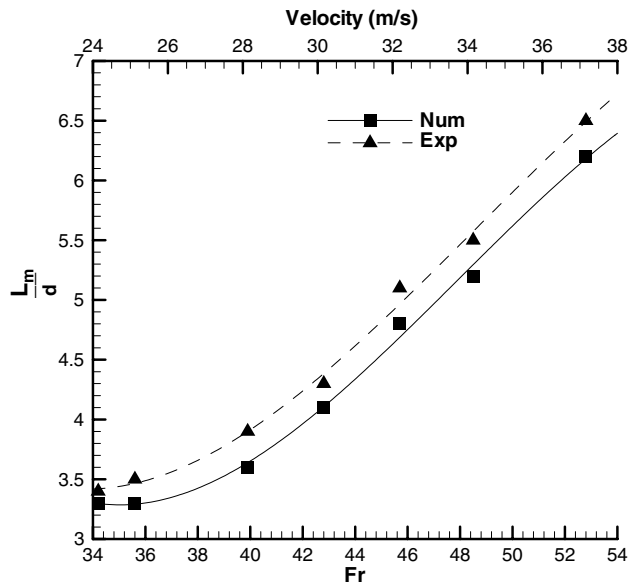


Fig. 12 Dimensionless cavity length versus Froude number

where  $d$  is the diameter of the cavitator and  $D$  and  $L$  are the maximum diameter and length of the cavity respectively. In Eq. (16),  $C_D$  is a parameter which depends on the cavitator geometry with a recommended value of 0.84 for disks and 0.26 for cones [29]. It should be mentioned that Reichardt's formulations are limited to  $\sigma < 0.12$  and natural cavitation, with the above equations being extrapolated to higher cavitation numbers in the present study.

Also, according to the application of Matched Asymptotic Expansions Method (MAEM), the empirical formulas for the vapor cavity diameter under small cavitation number were obtained [30]:

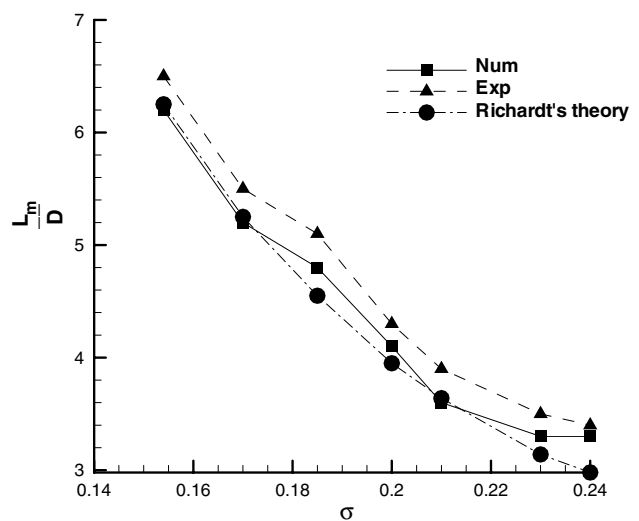
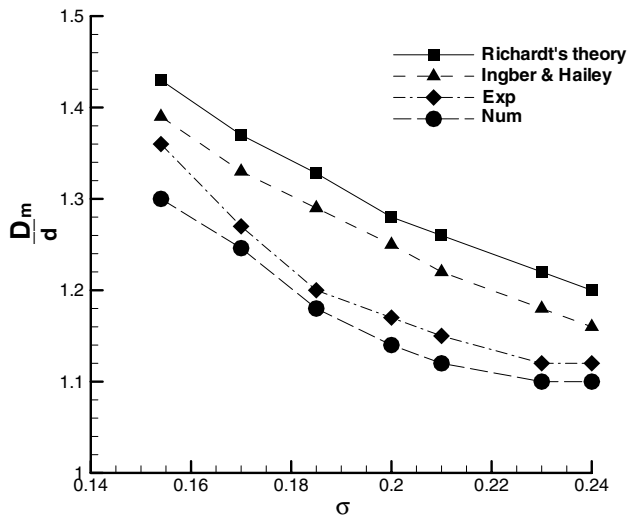


Fig. 14 The effect of cavitation numbers on dimensionless cavity length

$$\frac{D}{d} = \sqrt{\frac{C_{D_o}(1 + \sigma_v)}{\sigma_v}} \tag{17}$$

Figures 14 and 15 draw a comparison between the cavity length and diameter and that of the experimental data, numerical results and analytical relations reported by Reichardt [21]. The results show a maximum of 12 % difference between present results and those of Reichardt's theory reported for the cavity length. As discussed earlier, the reduced cavitation number leads to an increase in the length and diameter of the cavity.





**Fig. 15** The effect of cavitation numbers on dimensionless cavity diameter

The shape and dimensions of both natural and ventilated supercavitations are identical when the cavitation number is insignificant (Figs. 14, 15). According to Fig. 15, the maximum difference between present results and those of Reichardt and Ingber [30] for a cavity diameter is 10 and 8 % respectively.

According to the numerical predictions, cavity length can be increased by 150 % for low cavitation number, while a cavity length increase of 170 % is attained in higher cavitation condition (Table 1). According to the Fig. 16, the changes rate of cavity length is similar for both ventilated cavitation and natural cavitation. The length of ventilated cavity is almost equal to that of natural cavity for the same cavitation number, and the difference does not exceed 10 %. However, the variation rate of cavitation number is different for both ventilated cavitation and natural cavitation at various velocities.

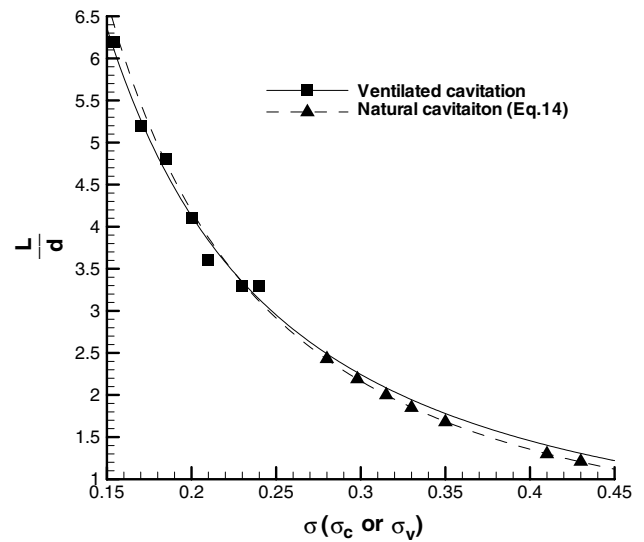


**Fig. 16** Comparisons of cavity length with and without ventilation

### 6.2 Drag coefficient

In this section, the drag force and drag coefficient are investigated for a 30° cavitator. Figure 17 shows the drag force of 30° cavitator for  $0.15 < \sigma < 0.24$ . Changes of drag force versus cavitation number are linear. It is observed that the drag coefficient declines steadily with an increase in the cavitation number. Figure 20 indicates the experimental and numerical drag coefficients versus Froude number. The Figs. 17 and 18 show a good qualitative agreement between the experimental and the numerical results derived from the finite element method. As shown in Fig. 18, the drag coefficient reduces as the Froude number rises.

According to Fig. 18, the drag coefficient increases initially and then remains at a constant level when Froude number drops, which is mainly due to the open end of cavity and the direct ejection of the ventilated air at  $v > 29$  m/s.

**Table 1** Comparison of Cavity length for natural and ventilated cavitation

Velocity flow (m/s)	Ventilated cavitation number	Natural cavitation number	for Ventilated cavitation(m)	Cavity length for Natural cavitation(m) (Eq. 14)
37	0.154	0.28	0.062	0.024
34	0.17	0.298	0.052	0.022
32	0.185	0.315	0.048	0.020
30	0.2	0.33	0.041	0.018
28	0.21	0.35	0.036	0.017
25	0.23	0.41	0.033	0.013
24	0.24	0.43	0.033	0.012

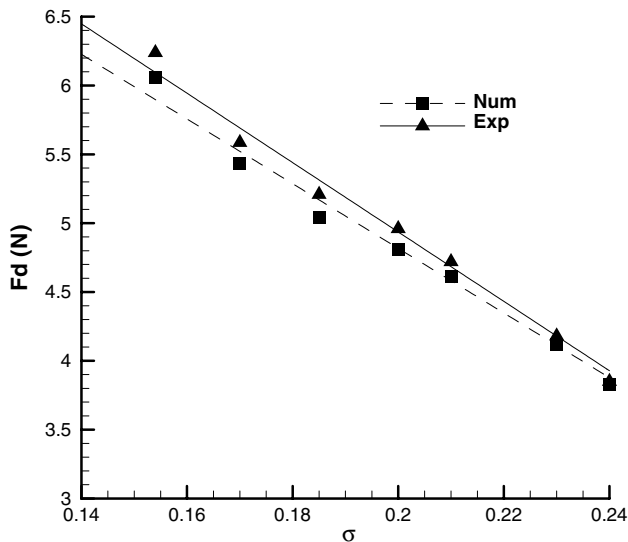


Fig. 17 Drag force variation with cavitation number

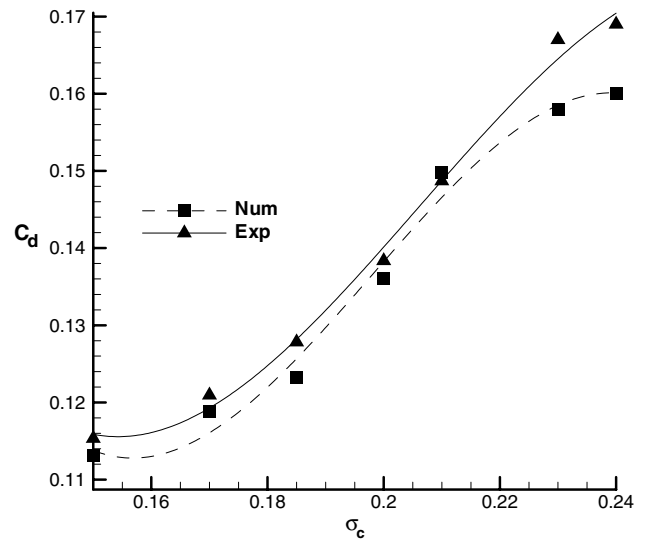


Fig. 19 The relationship between ventilated cavitation number and drag coefficient

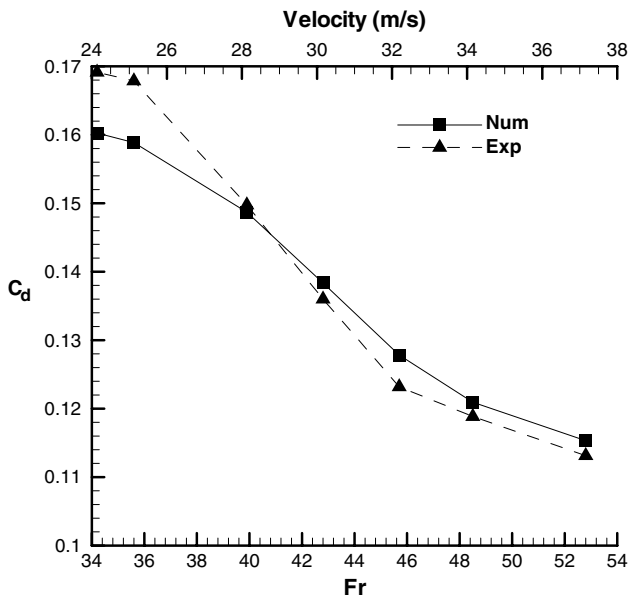


Fig. 18 Drag coefficient variation with Froude number

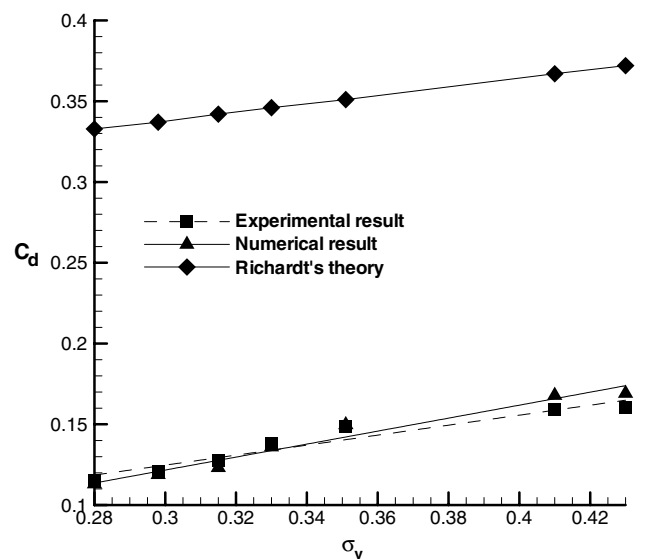


Fig. 20 Comparison of estimated drag coefficient with experimental data and Reichardt's theory

For this reason, at  $v < 29$  m/s, the drag coefficient variation is negligible.

The drag coefficient variation is also significantly influenced by the ventilated cavitation numbers, as it is less than 0.22. As shown in Fig. 19, the drag coefficient increases initially at a relatively fixed rate and it is then consolidated. This change of drag coefficient is consistent with the experimental results of Phillip [31] and the numerical result of Li-ping et al. [10]. Furthermore, with a reduction in the cavitation number, the pressure drag coefficient increases gradually and friction drag coefficient drops.

For a  $30^\circ$  cavitator, the total drag coefficient can be reduced to a minimum value with a cavity thickness to cavitator diameter ratio of about 0.016 or the ventilated cavitation number of 0.15.

In Fig. 19, the numerical drag coefficient is compared with the experimental data. A comparison of Figs. 19 and 20 shows that the variation of drag coefficient versus ventilated cavitation number is non-linear although the change of drag coefficient versus natural cavitation number is linear.

Figure 20 depicts the variation of drag coefficient with natural cavitation number. In this figure, the drag

coefficient is compared with the experimental data and the theoretical results provided by Reichardt [21] (Eq. 16). As shown in Fig. 20, the results indicate a maximum of 6 % difference between numerical and experimental results. The difference between present results and the theoretical data (mean = 80 %) is due to the fact that Reichardt's theory is valid for small cavitation numbers and natural cavitation.

For ventilated cavitation, the drag coefficient variation corresponds to the result of natural cavitation (Reichardt's theory). Thus, for the ventilated cavitation, drag coefficient variation with ventilated cavitation number is linear. At  $0.15 < \sigma_c < 0.25$  with an increase in the cavitation number, the drag coefficient rises to 50 %.

## 7 Conclusion

In this paper, a numerical and experimental analysis of the cavitating flow around a 30° cavitator was conducted. The experimental tests were carried out in a loop-water tunnel. The effects of flow velocity and cavitation number on cavity shape and drag coefficient were investigated.

The following conclusions can be drawn from the results of this study:

- For the ventilated cavitation simulation, there is a strong agreement between the predicted cavitation characteristics such as cavity length, cavity diameter and cavity shape and the analytic and experimental results.
- When the ventilated cavitation number is 0.15 or the ratio of cavity thickness to cavitator diameter is near 0.016, the drag coefficient of cavitator may be reduced to a minimum value.
- According to the numerical predictions, cavity length can be increased by 150 % for the lower cavitation number, while this value can reach as high as 170 % for higher cavitation condition.
- In other words, in higher cavitation numbers, ventilated cavitation has greater effect on increasing cavity length.
- Flow velocity has a less significant effect on the diameter of cavity. Thus, with an increase in the flow velocity, the cavity length and diameter increased by 200 and 18 % respectively.
- According to the results, the drag coefficient reduction in the ventilated cavitation (over 65 %) was greater than the natural cavitation.
- At constant rate of ventilated air, with an increase of the cavitation number from 0.15 to 0.25, the drag force is decreased by 62 %.
- In ventilated cavitation and after cavity closure, the length and diameter of cavity was less dependent on the flow velocity, although the rate of ventilated air had a significant effect on increasing the cavity length.
- Changes rate of cavity length is similar for both ventilated cavitation and natural cavitation. The length of ventilated cavity is almost equal to that of natural cavity at same cavitation number.

## References

- Lecoffre Y (1999) Cavitation Bubble Trackers. A.A. Balkema, Brookfield
- Zhang X, Wei Y, Zhang J, Wang C, Yu K (2007) Experimental research on the shape charates natural adn ventilated supercavitation. *J Hydrodyn Ser B* 19(5):564–571
- Wosnik M, Schauer T, Arndt R (2003) Experimental study of a ventilated supercavitating vehicle. 5th International Symposium on Cavitation. Osaka, Japan
- Savchenko YN, Semenenko VN (1998) The gas absorption into supercavity from liquid–gas bubble mixture. 3rd International symposium on cavitation. Grenoble, France, pp 49–53
- Feng X, Lu C, Hu T (2002) Experimental research on a supercavitating slender body of revolution with ventilation. *J Hydrodyn Ser B* 14(2):17–23
- Feng X, Lu C, Hu T, Wu L, Li J (2005) The fluctuation characteristics of natural and ventilated cavities on an axisymmetric body. *J Hydrodyn* 17(1):87–91
- Ji B, Luo X, Peng X, Zhang Y, Wu Y, Xu H (2010) Numerical investigation of the ventilated cavitating flow around an underwater vehicle based on a three-component cavitation model. *J Hydrodyn Ser B* 22(6):753–759
- Nesteruk I (2014) Shape of slender axisymmetric ventilated supercavities. *J Comput Eng* 2014:501590. doi:10.1155/2014/501590
- Rashidi I, Ma Passandideh-Fard, Mo Pasandideh-Fard, Nouri NM (2014) Numerical and experimental study of a ventilated supercavitating vehicle. *J Fluids Eng* 136(10):301–308
- Li-ping J, Cong W, Ying-Jie W (2006) Numerical simulation of artificial ventilated cavity. *J Hydrodyn* 18(3):273–279
- Javadpour M, Farahat S, Ajam H, Salari M, Hossein Nezhad A (2016) An experimental and numerical study of supercavitating flows around axisymmetric cavitators. *J Theor Appl Mech* 54(3):795–810
- Asnaghi A, Jahanbakhsh E, Saeed Seif M (2010) Unsteady multiphase modeling of cavitation around NACA 0015. *J Mar Sci Technol* 18(5):689–696
- Baradaran Fard M, Nikseresht AH (2012) Numerical simulation of unsteady 3D cavitating flows over axisymmetric cavitators. *Sci Iran B* 19(5):1258–1264
- Ji B, Luo X (2010) Numerical investigation of the ventilated cavitating flow around an under-water vehicle based on a three-component cavitation model. *J Hydrodyn Ser B* 22(6):753–759
- Jian-hong G, Chuan-jing L, Chen Ying C (2011) Characteristics of flow field around an underwater projectile with natural and ventilated cavitation. *J Shanghai Jiaotong Univ* 16(2):236–241
- Huang B, Wang GY (2011) Experimental and numerical investigation of unsteady cavitating flows through a 2D hydrofoil. *J Sci China Technol Sci* 54(7):1801–1812
- Zou W, Yu KP, Wan XH (2010) Research on the gas-leakage rate of unsteady ventilated supercavity. *J Hydrodyn* 22(5):778–783
- Zhou J, Yu K, Min X, Yang M (2012) The comparative of study of ventilated supercavity shape in water tunnel and infinite flow field. *J Hydrodyn Ser B* 22(5):689–696
- Kawakami E, Arndt RE (2011) Investigation of the behavior of ventilated supercavities. *J Fluids Eng* 133(9):09135
- Xin C, Chuan-jing L, Jie L, Zhan-cheng P (2008) The wall effect on ventilated cavitating flows in closed cavitation tunnels. *J Hydrodyn Ser B* 20(5):561–566

21. Franc JP, Michel JM (2004) *Fundamentals of cavitation*. Kluwer Academic Publisher, Dordrecht, Netherlands
22. Semenenko VN (2001) Dynamic processes of supercavitation and computer simulation, In Paper presented at the RTO AVT lecture series on supercavitating flows at VKI. 2001
23. Menter FR. (1993) Zonal two equation  $k$ - $\omega$  turbulence models for aerodynamic flows. AIAA Fluid Dynamics Conference; 24th; 6–9 Jul. Orlando, United States
24. Li Z, Pourquie P, Terwisga VA (2010) Numerical study of steady and unsteady cavitation on a 2d hydrofoil. *J Hydrodyn Ser B* 22(5):770–777
25. Singhal AK, Athavale MM, Li H, Jiang Y (2002) Mathematical basis and validation of the full cavitation model. *J Fluids Eng* 124:617–624
26. Merkle CL, Feng J, Buelow P (1998) Computational modeling of the dynamics of sheet cavitation. In: *Proceeding of the 3rd international symposium on cavitation*. Grenoble, France
27. Schnerr G, Sauer J (2001) Physical and numerical modeling of unsteady cavitation dynamics. In: *Proceedings of the 4th international conference on multiphase Flow*, New Orleans, LA, USA
28. Kunz RF, Boger DA, Chyczewski TS, Stinebring DR, Gibeling HJ, Govindan TR (1999) Multi-phase CFD analysis of natural and ventilated cavitation about submerged bodies. In: *3rd ASME/JSME Joint Fluids Engineering Conference*. San Francisco, California
29. Rouse H, McNown JS (1948) Cavitation and pressure distribution, head forms at zero angle of yaw, in *studies in engineering, bulletin*, 32. State University of Iowa Aemes, Iowa
30. Ingber MS, Hailey CE (1992) Numerical modeling of cavities on axisymmetric bodies at zero and non-zero angle of attack. *J Numer Methods Fluid* 15:251–271
31. Phillip B (1993) Experimental study of a ventilated supercavitating vehicle. *J Fluid Mech* 254:131–150